Biochimica et Biophysica Acta 1853 (2015) 1395–1405

Contents lists available at ScienceDirect

Biochimica et Biophysica Acta

journal homepage: www.elsevier.com/locate/bbamcr

Review

Mössbauer spectroscopy of Fe/S proteins ☆,☆☆

Maria-Eirini Pandelia [a,*], Nicholas D. Lanz [b], Squire J. Booker [a,b], Carsten Krebs [a,b,**]

[a] Department of Chemistry, The Pennsylvania State University, University Park, PA, USA 16802
[b] Department of Biochemistry and Molecular Biology, The Pennsylvania State University, University Park, PA, USA 16802

ARTICLE INFO

Article history:
Received 18 September 2014
Received in revised form 17 November 2014
Accepted 3 December 2014
Available online 10 December 2014

Keywords:
Mossbauer spectroscopy
EPR spectroscopy
Fe/S clusters

ABSTRACT

Iron-sulfur (Fe/S) clusters are structurally and functionally diverse cofactors that are found in all domains of life. ^{57}Fe Mössbauer spectroscopy is a technique that provides information about the chemical nature of all chemically distinct Fe species contained in a sample, such as Fe oxidation and spin state, nuclearity of a cluster with more than one metal ion, electron spin ground state of the cluster, and delocalization properties in mixed-valent clusters. Moreover, the technique allows for quantitation of all Fe species, when it is used in conjunction with electron paramagnetic resonance (EPR) spectroscopy and analytical methods. ^{57}Fe-Mössbauer spectroscopy played a pivotal role in unraveling the electronic structures of the "well-established" [2Fe-2S]$^{2+/+}$, [3Fe-4S]$^{1+/0}$, and [4Fe-4S]$^{3+/2+/1+/0}$ clusters and -more-recently- was used to characterize novel Fe/S clustsers, including the [4Fe-3S] cluster of the O_2-tolerant hydrogenase from *Aquifex aeolicus* and the 3Fe-cluster intermediate observed during the reaction of lipoyl synthase, a member of the radical SAM enzyme superfamily.

1. Introduction

Iron-sulfur (Fe/S) clusters are one of the most ubiquitous cofactors in nature and are widespread among organisms from all three domains of life. Their basic building block consists of an Fe ion in, with a few exceptions, a distorted tetrahedral symmetry coordinated by inorganic sulfides (S^{2-}) and protein-based ligands (most often the thiolate of a cysteine residue) [1–3]. The structural and redox plasticity of Fe/S cofactors allows for a very diverse functional repertoire, ranging from electron transfer, non-redox and redox catalysis -most notably represented by the superfamily of radical *S*-adenosyl-L-methionine (SAM)-dependent enzymes that functionalize C-H bonds-, O_2-sensing, regulation, and structural roles in enzymes involved in DNA replication and protein biosynthesis [4–11]. Due to the rapid progress of genomic sequencing, an abundance of novel putative Fe/S-containing proteins with unknown functions are continuously being discovered. Because prediction of the number and type(s) of Fe/S cluster(s) solely from protein sequences is not reliable, sensitive spectroscopic methods are required for their identification and characterization.

Of the many spectroscopic techniques that are routinely used to characterize Fe/S clusters, ^{57}Fe-Mössbauer plays a pivotal role for the following reasons [12,13]. First, *all* chemically distinct ^{57}Fe-labeled species in the sample are detected, irrespective of their oxidation and spin states. Second, the Mössbauer spectrum is the weighted superposition of the individual subspectra of the various Fe sites contained in the sample. Importantly, the relative area of a given subspectrum is proportional to the relative concentration of the corresponding Fe species. Third, Fe/S clusters have unique Mössbauer-spectroscopic properties that allow for their identification and detailed characterization of their electronic and geometric structures.

^{57}Fe-Mössbauer spectroscopy is even more powerful when combined with Electron Paramagnetic Resonance (EPR) spectroscopy, a technique that is widely used to characterize Fe/S clusters, because the two methods rely on the same theoretical concept (the spin Hamiltonian formalism) to describe the spectral features, as well as analytical methods to determine the Fe:protein stoichiometry [14,15]. Such a combined approach represents the most rigorous method for establishing the types and stoichiometry of various Fe-containing cofactors in a given protein.

2. Brief introduction to Mössbauer spectroscopy

The Mössbauer effect is the *recoilless* resonance absorption and emission of nuclear γ irradiation [13,16,17]. While the effect has been observed for about 80 nuclides of 43 different elements, it is mostly applied to studies of the isotope ^{57}Fe, a stable isotope with natural abundance of 2.1% [13]. The γ-photon used for ^{57}Fe Mössbauer spectroscopy results from the radioactive decay of the ^{57}Co isotope, which

☆ This work was supported by NIH Grants GM-63847 and GM-103268 (S.J.B.), the Dreyfus Foundation (Teacher Scholar Award to C.K.), and the Beckman Foundation (Young Investigator Award to C.K.).
☆☆ This article is part of a Special Issue entitled: Fe/S proteins: Analysis, structure, function, biogenesis and diseases.
* Correspondence to: M.-E. Pandelia, 317 Chemistry Building, The Pennsylvania State University, University Park, PA 16802. Tel.: +1 814 863 0484; fax: +1 814 865 2927.
** Correspondence to: C. Krebs, 332 Chemistry Building, The Pennsylvania State University, University Park, PA 16802. Tel.: +1 814 865 6089; fax: +1 814 865 2927.
E-mail addresses: mxp65@psu.edu (M.-E. Pandelia), ckrebs@psu.edu (C. Krebs).

http://dx.doi.org/10.1016/j.bbamcr.2014.12.005
0167-4889/

has a half-life of 271.8 days (Fig. 1A) and yields a metastable ^{57}Fe state that decays to the ground state via a series of transitions. For ^{57}Fe Mössbauer spectroscopy the 14.4-keV photon emitted from the first excited nuclear state ($I = 3/2$) is used. This emitted photon can then be absorbed by a ^{57}Fe nucleus in the sample in the ground state ($I = 1/2$), thereby promoting it to the first excited state. Emission and absorption lines have a finite linewidth that is determined by the lifetime of the exited state, through Heisenberg's uncertainty principle; the mean lifetime of the $I = 3/2$ excited state of ^{57}Fe is $1.47 \cdot 10^{-7}$ s [18].

Absorption and emission of a γ-photon significantly shift the energy of the absorbed and emitted γ-photon due to recoil, and because the energy shift is approximately 5 orders of magnitude greater than the intrinsic linewidth of the ^{57}Fe excited state, the effect can only be observed for *recoilless* absorption and emission of the γ-photon. Rudolf Mössbauer showed that there is a finite probability *f* for recoilless absorption and emission if both emitter and absorber are embedded in a solid matrix. Therefore, Mössbauer spectra of proteins are typically collected on frozen solutions. The *f* factor (also known as Lamb-Mössbauer factor) is proportional to the mean square displacement of the ^{57}Fe nucleus and as a consequence decreases monotonically with increasing temperature [13]. Because *f* is approximately 0.8 at 4.2 K for all ^{57}Fe species irrespective of their chemical form, the experimentally observed Mössbauer spectrum is the superposition of the subspectra of all ^{57}Fe-labeled species in the sample, weighted according to their relative concentrations [13,17]. Thus, Mössbauer spectroscopy can be used to quantify the various ^{57}Fe-labeled species in a sample. Typical requirements for biological samples of Fe-containing proteins are volumes of 250 - 400 μL and ^{57}Fe concentrations of 1−5 mM [12]. Although some biological materials with natural abundance Fe have been studied by Mössbauer spectroscopy, it is generally required that samples be enriched with ^{57}Fe. An important consideration for studies of Fe/S clusters by Mössbauer spectroscopy is that the commonly used reconstitution methods with Fe and sulfide often result in poorly defined Fe/sulfide contaminants that can bind to the protein. If these contaminants are not removed (e.g. by gel filtration chromatography), their contribution to the Mössbauer spectra will impede analysis and interpretation [14].

The layout of a Mössbauer spectrometer follows the concept of all transmission spectroscopic techniques [13]; a source produces the γ-photons, a sample enriched with the ^{57}Fe isotope absorbs the γ-irradiation and a proportional detector converts the γ-photons after the absorption event to electric pulses. Because the emitter (source) and absorber (sample) are chemically distinct, the energies of the ground and excited nuclear states are perturbed differently. As a consequence, a range of energies must be scanned for the Mössbauer event (i.e. resonance absorption) to be observed. The energy of the emitted γ-photon is modulated using the Doppler effect according to the following formula, in which *v* is the Doppler velocity and *c* is the speed of light:

$$\Delta E = (v/c)\, E_\gamma$$

Recording of a Mössbauer spectrum thus involves synchronization of the source velocity to the counting of the photons. In a Mössbauer spectrum, the source velocity is displayed on the x-axis, while the fraction of photons transmitted through the sample is shown on the y-axis. For the calibration of the energy scale of a Mössbauer spectrometer, the spectrum of a standard absorber with known hyperfine splitting is recorded. Most commonly a thin foil of metallic α-iron at room temperature is used for this purpose [13]. Virtually all chemically distinct forms of ^{57}Fe will absorb within a narrow range of energies corresponding to Doppler velocities of approximately −12 mm/s to +12 mm/s.

2.1. Chemical information obtainable from Mössbauer Spectra

The simplest type of Mössbauer spectrum is referred to as quadrupole doublet (Fig. 1B). The two lines of a quadrupole doublet correspond to transitions from the $I = 1/2$ ground state to the $M_I = \pm 1/2$ and $\pm 3/2$ states of the $I = 3/2$ excited nuclear state, respectively. A quadrupole doublet is characterized by the following two parameters: the isomer shift, δ, which is given by the average position of the two lines with respect to the zero velocity point, and the quadrupole splitting parameter, ΔE_Q, which is given by the separation of the two lines. Both parameters are quoted in velocity units (mm/s). When the ^{57}Fe nucleus experiences a magnetic field, the nuclear levels of the ground and excited states split due to the nuclear Zeeman effect, resulting in magnetically split spectra, which are more complex and depend on many more parameters (*vide infra*).

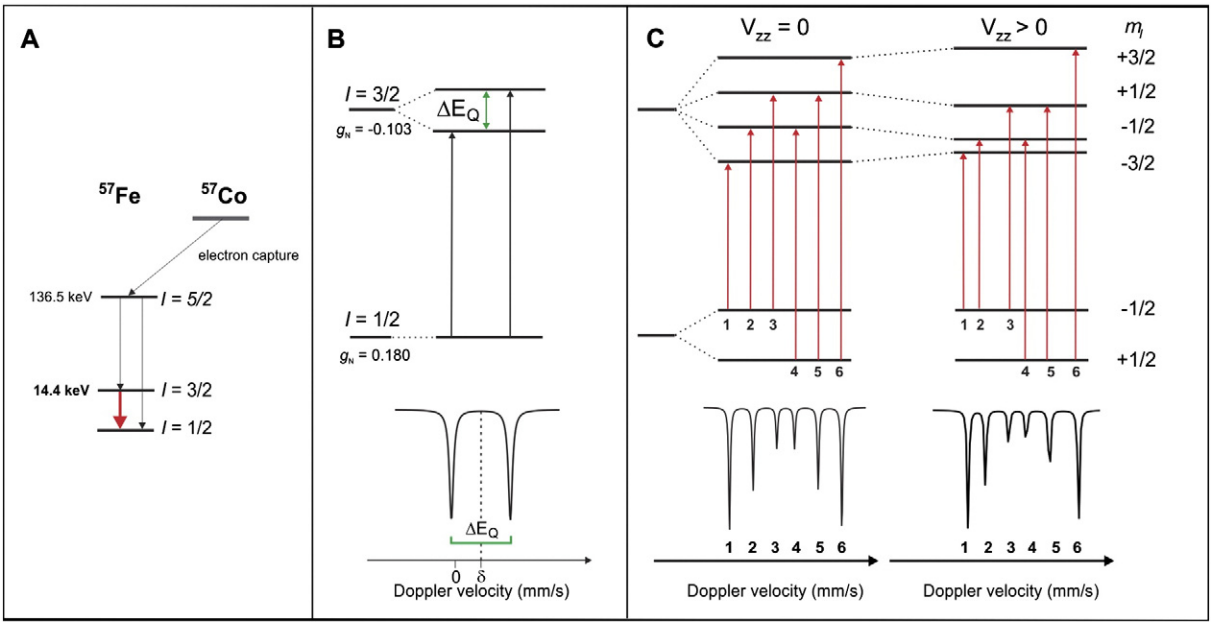

Fig. 1. (**A**) Decay scheme of the ^{57}Co to ^{57}Fe and the respective ^{57}Fe nuclear transitions (**B**) Mössbauer transitions in the absence of an applied magnetic field and the corresponding quadrupole spectrum they give rise to. (**C**) Mössbauer transitions in the presence of a magnetic field $\mathbf{B}_{eff}$ (see text) and the six-line magnetically-split spectrum they give rise to in the absence ($V_{zz} = 0$) and presence ($V_{zz} > 0$) of a first order quadrupole interaction due to EFG.

2.1.1. Isomer shift

The isomer shift (δ) also referred to as the electric monopole interaction, arises from the Coulomb interaction between nuclear and electric charge distributions, and leads to changes in the nuclear energy levels. Assuming that the nucleus is a charged sphere of radius R and the electronic charge density is $e\psi(0)^2$, δ is given as:

$$\delta = \frac{4\pi}{5} Ze^2 \left\{ |\psi(0)|_A^2 - |\psi(0)|_S^2 \right\} \cdot R^2 \left(\frac{\Delta R}{R} \right)$$

where the subscript S denotes the sample and A the absorber, and $\Delta R = R_e - R_g$ is the difference between the radii of the first exited (e) and ground state (g) of ^{57}Fe [13,19].

The isomer shift provides a measure of the *s*-electron density at the ^{57}Fe nucleus and is influenced by the *p* and *d* electrons by means of electrostatic shielding. It is also influenced by valence 4 s electrons that participate in bonding and thus lead to significant isomer shift variations [13]. Because ΔR is negative for ^{57}Fe, a more positive isomer shift implies a lower electron density at the nucleus. δ is sensitive to the formal oxidation state, the spin state, the number and the type of ligands, as well as the covalency of the Fe-ligand bonds. The following trends help for the interpretation of Mössbauer isomer shifts: (i) $\delta(Fe^{IV}) < \delta(Fe^{III}) < \delta(Fe^{II})$, (ii) $\delta_{high\text{-}spin} > \delta_{low\text{-}spin}$, (iii) soft ligands cause lower isomer shifts than more ionic ligands because of the increased covalency of the Fe-ligand bond, and (iv) six coordinate complexes have higher isomer shifts (because of their less covalent bond) than four coordinate complexes [13]. The isomer shift has a temperature-dependent term due to relativistic contributions, also known as second-order Doppler shift (δ_{SOD}) [13]. Therefore, it is important to compare isomer shifts of different compounds obtained from spectra collected at the same temperature.

2.1.2. Nuclear quadrupole interaction

The nuclear excited $I = 3/2$ state has a non-spherical charge distribution and produces a quadrupole moment that can interact with the inhomogeneous electric field at the ^{57}Fe nucleus, described by the electric field gradient (EFG). This interaction causes splitting of the nuclear energy levels into two substates with quantum numbers $M_I = \pm 1/2$, $M_I = \pm 3/2$ (Fig. 1), giving rise to the two lines of the quadrupole doublet. The separation between the two peaks of the doublet is called quadrupole splitting ΔE_Q and is given as:

$$\Delta E_Q = \frac{1}{2} eQV_{zz} \sqrt{1 + \frac{\eta^2}{3}}$$

in which e is the elementary charge, Q is the quadrupole moment of the excited state of ^{57}Fe, V_{zz} is the z-component of the EFG, and η is the asymmetry parameter defined as $\eta = \frac{V_{xx} - V_{yy}}{V_{zz}}$. ΔE_Q typically reflects the population of the iron 3d orbitals as well as the (a)symmetry of the ligand charges surrounding the ^{57}Fe nucleus. The determination of the sign of ΔE_Q and of the asymmetry parameter η typically requires measurements in externally applied fields and/or at different temperatures [13,17].

2.1.3. Magnetic hyperfine interactions

The magnetic properties of mononuclear, paramagnetic transition metal complexes are typically described by means of the spin Hamiltonian formalism:

$$H_{el} = \beta \mathbf{S} \cdot \mathbf{g} \cdot \mathbf{B} + D \left[\mathbf{S_z^2} - \frac{1}{3} S(S+1) + \frac{E}{D} \left(\mathbf{S_x^2} - \mathbf{S_y^2} \right) \right] + \mathbf{S} \cdot \mathbf{A} \cdot \mathbf{I}$$

The first term represents the electronic Zeeman effect, which describes the interaction of the electron spin, **S**, with the magnetic field, **B**, and is characterized by the **g**-tensor. The **g**-tensor has three principal components, g_x, g_y, and g_z, which can deviate significantly from the free-electron g-value, $g_e = 2.0023$, due to spin-orbit coupling. The second term describes the zero-field splitting (ZFS) interaction and originates from second-order perturbation treatment of the interaction of spin and orbital angular momenta [20]. It is parameterized with the axial ZFS parameter, D, and the rhombicity parameter, E/D. For systems with $S \geq 1$ this interaction lifts the $(2S + 1)$-fold degeneracy in zero applied magnetic field. The last term is known as the hyperfine interaction and parameterizes the interaction between the electronic spin **S** and nuclear spin **I** through the hyperfine coupling tensor **A**.

This Hamiltonian is commonly used as the basis for the analysis of EPR and Mössbauer spectra. The difference, however, is that by EPR spectroscopy the electron spin system properties are directly probed, whereas by Mössbauer spectroscopy they are sensed indirectly via the hyperfine interaction, which perturbs the energy levels of the nuclear levels of the ground and excited states of ^{57}Fe. For the calculation of Mössbauer spectra, it is customary to calculate the properties of the electron spin system, taking into account electron Zeeman and ZFS terms. From the solution one can calculate the so-called spin expectation value, $\langle \mathbf{S} \rangle$, and substitute it for **S** in the hyperfine term in the following nuclear Hamiltonian [13,17,19]:

$$H_{nuc} = -g_N \mu_N \left[\frac{-\langle \mathbf{S} \rangle \cdot \mathbf{A}}{g_N \beta_N} + \mathbf{B}_{ext} \right] \cdot \mathbf{I} + \mathbf{I} \cdot \mathbf{Q} \cdot \mathbf{I}$$

in which the first term represents the effective hyperfine coupling, the second term represents the nuclear Zeeman effect of ^{57}Fe, and the last term represents the quadrupole interaction (see above). Importantly, the hyperfine term, divided by $g_N\beta_N$ has units of magnetic field and it is commonly referred to as the internal magnetic field:

$$\mathbf{B_{int}} = \frac{-\langle \mathbf{S} \rangle \cdot \mathbf{A} \cdot \mathbf{I}}{g_N \beta_N}$$

where g_N is the nuclear g-value of the ^{57}Fe ground state and β_N is the nuclear magneton.

The effective magnetic field experienced by the ^{57}Fe nucleus is the sum of the external and internal fields: $\mathbf{B}_{eff} = \mathbf{B}_{ext} + \mathbf{B}_{int}$ and perturbs the energy of the nuclear levels of the ground and excited states due to the nuclear Zeeman effect (Fig. 1). The six magnetic dipole allowed transitions ($\Delta M_I = 0, \pm 1$) for the ^{57}Fe nucleus are shown in Fig. 1C [13,16]. The intensity ratio of the $\Delta M_I = \pm 1$ lines and $\Delta M_I = 0$ lines depends on the relative orientation of $\mathbf{B}_{eff}$ to the propagation direction of the γ-beam [13,17]. Importantly, the magnitude of the splitting depends on the magnitude of $\mathbf{B}_{eff}$. Therefore, one can determine $\mathbf{B}_{eff}$ from analysis of magnetically split spectra. Because $\mathbf{B}_{ext}$ is known for the experiment, one can deduce $\mathbf{B}_{int}$. Analysis of Mössbauer spectra collected in variable external magnetic fields allows for determination of the properties of the electron spin ground state (**S**, **g**, D, and E/D), as well as the magnitude and sign of **A**. The **A**-tensor for ^{57}Fe is dominated by the Fermi contact term, which typically has values of $A/g_N\beta_N$ of -20 to -22 T (in magnetic field units) or A = -27 to -30 MHz (in frequency units; the conversion factor is 1.38152 T/MHz for the ground state of the ^{57}Fe nucleus).

For reasons that go beyond the scope of this article, one needs to distinguish the EPR and Mössbauer properties of Fe species with half-integer spin ground state or Kramers systems (i.e. $S = 1/2, 3/2, 5/2$, etc), from those of Fe species with integer-spin ground state or non-Kramers systems (i.e. $S = 0, 1, 2$, etc) [15,17]. Complexes with half-integer spin ground state typically give rise to signals in EPR spectroscopy in perpendicular mode and exhibit typically magnetically split Mössbauer spectra that are governed by large $\mathbf{B}_{int}$. The analysis of such Mössbauer spectra is often complex, but the parameters of the electron spin ground state (**S**, **g**, D, E/D) can often be obtained independently from EPR. Conversely, Fe complexes with integer spin ground state often (but not always) do not give rise to EPR signals in perpendicular

mode. These non-Kramers systems, however, can give rise either to quadrupole doublet features in weak applied fields or magnetically broadened components that coalesce into doublets without applied magnetic field. In both cases, the Mössbauer spectra provide valuable information about the electronic properties of the system, which is nicely complemented by EPR spectroscopy to allow for the complete characterization of the Fe complexes. The $[3Fe\text{-}4S]^0$ and $[4Fe\text{-}4S]^0$ clusters serve as excellent examples for the complementary nature of the two methods for the analysis for systems with integer-spin ground states [21–23].

Electronic relaxation between two electronic transition states occurs with a relaxation time τ and is an important factor that markedly affects the Mössbauer spectra of paramagnetic Fe species [18,19]. In this respect, two extreme cases are usually considered for analysis and interpretation of the spectra: the electronic relaxation rate is much slower compared to the nuclear Larmor precession frequency ('slow relaxation limit', typically encountered at 4.2 K for metalloproteins) or much faster compared to the nuclear Larmor precession frequency ('fast relaxation limit', typically encountered at high temperatures). In the case of 'fast relaxation', $\langle \mathbf{S} \rangle$ is calculated for all states and averaged according to the Boltzmann population factors of the various states to yield $\langle \mathbf{S}_{av} \rangle$. Because $\langle \mathbf{S}_{av} \rangle$ is nearly zero in weak applied fields, the associated Mössbauer spectrum is a quadrupole doublet from which δ and ΔE_Q can be directly determined. In the case of the 'slow relaxation' regime, each electronic state will give rise to a magnetically split Mössbauer subspectrum. The various states have different $\mathbf{B}_{int}$ thus yielding distinct Mössbauer subspectra. The overall Mössbauer spectrum in the 'slow relaxation' regime is then the superposition of the Mössbauer subspectra of the various states, weighted according to the Boltzmann population factors [13,17,19].

2.1.4. Mössbauer properties of polynuclear clusters

Another important contribution to the electronic structure of complexes with two or more paramagnetic centers concerns the interaction between the two or more spins of the cluster. The dominant contribution to this interaction is the isotropic exchange coupling, which is mediated via the bridging ligands. Coupling of two spins $\mathbf{S}_1$ and $\mathbf{S}_2$ yields states with total spin $\mathbf{S}_{tot}$ that can take values from $|S_1 - S_2|$, $|S_1 - S_2 + 1|$,..., $|S_1 + S_2|$. The interaction can be parameterized by the Heisenberg-Dirac-van Vleck (HDvV) Hamiltonian, $H_{exchange} = J\ \mathbf{S_1}\cdot\mathbf{S_2}$[1] and the energies of the states with total spin S_{tot} are given as $E(S) = (J/2)\ S\cdot(S+1)$ [24,25]. For $J > 0$, the state with lowest value of S_{tot} is the ground state and this case is referred to as antiferromagnetic (AF) coupling, whereas for $J < 0$, the state with maximum value of S_{tot} is the ground state and this case is referred to as ferromagnetic (F) coupling.

In the following, we use the oxidized and reduced forms of a [2Fe-2S] ferredoxin to illustrate how exchange coupling affects the electronic structure of an exchange-coupled cluster, and how it can be probed by EPR and Mössbauer spectroscopies. Oxidized $[2Fe\text{-}2S]^{2+}$ clusters (left column in Fig. 2) contain two AF-coupled high-spin (HS) Fe^{III} ions ($S_1 = S_2 = 5/2$), yielding a diamagnetic $S_{tot} = 0$ ground state (EPR-silent). The Mössbauer spectrum of this cluster form exhibits one quadrupole doublet. It is worth noting that the two Fe^{III} sites are chemically distinct, each giving rise to its own subspectrum, but because the chemical environment of both sites is virtually identical, the features are not resolved. The Mössbauer parameters are typical for HS Fe^{III} S_4 centers with $\delta \sim 0.27$ mm/s.

Reduced $[2Fe\text{-}2S]^{+}$ clusters (right column in Fig. 2) contain one HS Fe^{III} site ($S_1 = 5/2$) AF-coupled to a HS Fe^{II} site ($S_2 = 2$) yielding a $S_{tot} = 1/2$ ground state (EPR-active). The Mössbauer spectra can be understood as the superposition of two equal intensity components, associated with the Fe^{III} (blue subspectra) and Fe^{II} (red subspectra) sites, respectively. At low temperature (4.2 K) and in a weak applied field

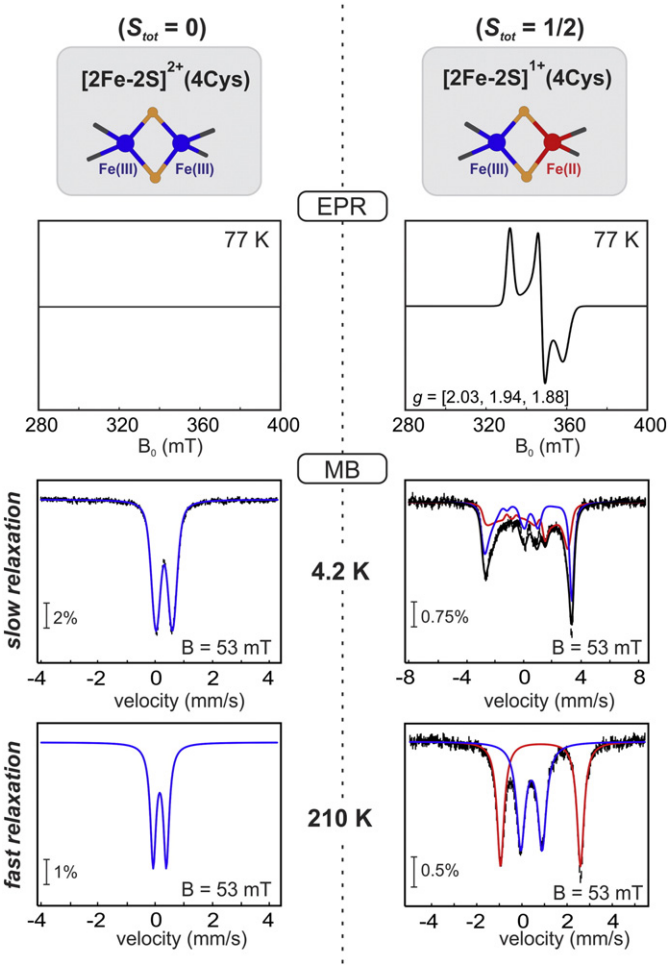

Fig. 2. Electronic properties and corresponding EPR and Mössbauer spectra of the oxidized and reduced all-cysteine ligated [2Fe-2S] ferredoxins. Mössbauer spectra at 4.2 K and 210 K were calculated in the "slow" and "fast" relaxation limit, respectively. Fe^{III} and Fe^{II} sites are shown in blue and red, respectively. Adapted from ref. [27].

(53 mT), each Fe site gives rise to a magnetically split subspectrum, because the fluctuation rate of the electron spin is slow compared to the ^{57}Fe Larmor frequency (slow relaxation limit). The observed magnetic splitting of the two subspectra is dominated by $\mathbf{B}_{int}$. As described in detail elsewhere [13,17,26], the internal field can be expressed with respect to the total spin of the cluster, $S_{tot} = 1/2$, or it can be expressed with respect to the local spin of the i-th Fe ion, S_i, according to the following equation:

$$\mathbf{B_{int}} = \frac{-\langle \mathbf{S_{tot}} \rangle \cdot \mathbf{A_{tot}} \cdot \mathbf{I}_i}{g_N \beta_N} = \frac{-\langle \mathbf{S_i} \rangle \cdot \mathbf{A_i} \cdot \mathbf{I}_i}{g_N \beta_N}$$

in which $\mathbf{A}_{tot}$ and $\mathbf{A}_i$ are related by the spin projection factor, $c_{i,S}$, according to

$$c_{i,S} = \frac{S(S+1) + S_i(S_i+1) - S_j\left(S_j+1\right)}{2S(S+1)}$$

For the $S_{tot} = 1/2$ state, the spin projection factors are $c_1 = +7/3$ and $c_2 = -4/3$ for the Fe^{III} and Fe^{II} sites, respectively. The different sign of c_1 and c_2 reflects the different orientation of the two spins in the ground state and thus translates into a different sign of the internal field of the two Fe sites, which has a distinctive impact on the Mössbauer spectra. For the site with positive c, $\mathbf{B}_{eff}$ decreases with increasing $\mathbf{B}_{ext}$ (spectral lines move inwards). By contrast, for the site with negative c, $\mathbf{B}_{eff}$ increases with increasing $\mathbf{B}_{ext}$ (spectral lines move

[1] Note also that other forms of the HDvV Hamiltonian operator are used in the literature: $-2J\ \mathbf{S_1}\cdot\mathbf{S_2}$, $-J\ \mathbf{S_1}\cdot\mathbf{S_2}$, for which the J-values differ by a factor of -2 and -1, respectively.

outwards). This field-strength dependence is nicely observable in spectra collected at variable $\mathbf{B}_{ext}$. In the high-temperature/weak-field Mössbauer spectrum the magnetically split features collapse to two quadrupole doublets, because the fluctuation rate of the electron spin is fast compared to the ^{57}Fe Larmor frequency (fast relaxation limit) and under these conditions, the thermally averaged $\langle \mathbf{S} \rangle$ is essentially zero. The Mössbauer parameters of the two sites are typical of HS Fe^{III} and HS Fe^{II} sites in tetrahedral S_4 ligand environment.

3. The geometric and electronic structures of common Fe/S clusters

The most common configurations of Fe/S cofactors in proteins are [2Fe-2S], cuboidal [3Fe-4S], and [4Fe-4S] clusters [4]. We adopt in the following the nomenclature used by most biochemists for Fe/S clusters, in which we indicate the total charge of the inorganic core, i.e. without accounting for the charges of the protein-derived or substrate-derived ligands. In all cases, the Fe ions are formally in the + III or + II oxidation state and are typically in a distorted tetrahedral coordination environment. Because this ligand field is weak, the Fe ions are in the HS configuration. In polynuclear clusters the individual spins of the Fe ions are coupled to yield the total spin state (S_{tot}) of the cluster (Fig. 3) [4,25,28,29]. The overall spin-state of an Fe/S cluster depends on the interplay between three interactions [21,28–32]: (i) Exchange coupling described by the HDvV Hamiltonian (see above); (ii) spin-dependent delocalization or double exchange B, which is observed in symmetric mixed-valent $(Fe^{2.5+})_2$ dimers, in which the extra electron is delocalized over a $(Fe^{III})_2$ moiety, and favors parallel alignment of spins; and (iii) vibronic coupling (VC) and solvent effects, which introduce static asymmetries and thus favor valence trapping and AF spin coupling.

In particular, the electronic structures of [3Fe-4S] and [4Fe-4S] clusters are very complex due to the large number of S_{tot} states with similar energies. The analysis of variable-field Mössbauer spectra with respect to the total electron spin ground state S_{tot} of the cluster often (but not always) allows for the determination of $\mathbf{A}_{tot}$ for the various Fe sites. Knowing the intrinsic A_i values determined for rubredoxin-like sites, $A(Fe^{2+}) = -38$ MHz, $A(Fe^{2.5+}) = -32$ MHz and $A(Fe^{3+}) = -31$ MHz [33], it is then possible to deduce the spin projection factors c_i and compare them to those predicted for possible spin coupling schemes.

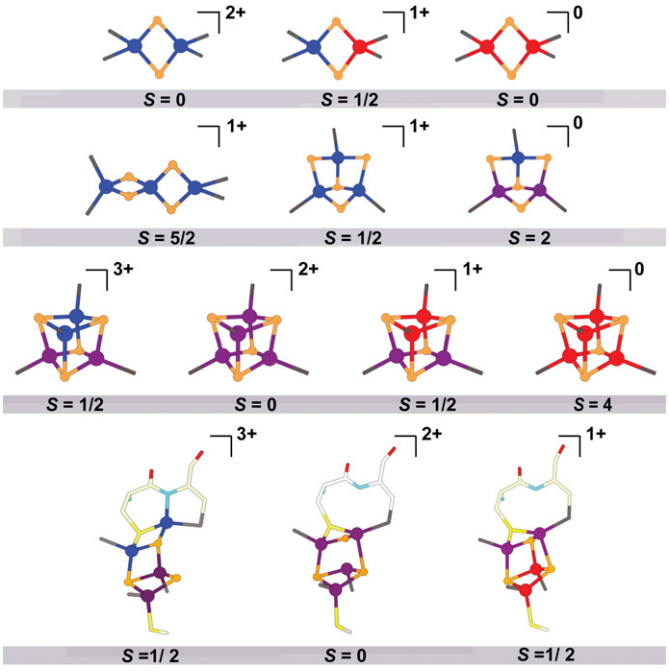

Fig. 3. Most important types of Fe/S clusters encountered in nature and their corresponding electronic properties. Fe^{III} is represented with blue, Fe^{II} with red and the mixed-valent $Fe^{2.5+}$ with purple spheres. Sulfide ligands are depicted with yellow spheres.

Mössbauer spectroscopy has served a pivotal role for understanding and establishing the intricate electronic structure of Fe/S clusters [4]. The careful analysis of the Mössbauer isomer shift δ, which is a sensitive measure of the Fe oxidation state, observed for the various Fe/S cluster forms laid the foundation for the understanding of their electronic structures. In particular the realization that Fe sites with isomer shift values between those typical of $Fe^{III}S_4$ and $Fe^{II}S_4$ sites reflect valence-delocalized $(Fe^{2.5+})_2$ pairs was a breakthrough for the understanding of their electronic structures [21,34,35].

From a more mundane point of view, the fact that the two most prevalent Fe/S clusters, the $[4Fe\text{-}4S]^{2+}$ and $[2Fe\text{-}2S]^{2+}$ forms have EPR-silent $S = 0$ ground states that exhibit diagnostic Mössbauer quadrupole doublet features that are relatively straightforward to identify and quantify, make Mössbauer spectroscopy an indispensable tool for studies of Fe/S proteins [14].

3.1. [2Fe-2S] clusters

[2Fe-2S] clusters occur in the 2 +, 1 + and 0 oxidation states (Fig. 3) and are usually subdivided into three subclasses: the Cys_4 ligated clusters [36], the Cys_2/His_2 Rieske clusters [37] and the more recently identified Cys_3/(His/Arg) [2Fe-2S] clusters [38,39]. The $[2Fe\text{-}2S]^{2+}$ form consists of two high-spin ferric ions AF-coupled to yield a diamagnetic ground state ($S_{tot} = 0$) and has isomer shifts of ~0.27 mm/s (Table 1). In the case of the His_2-ligated Rieske clusters, the sites are resolved due to the different coordination environments, with the His_2-coordinated Fe^{III} site exhibiting a larger ΔE_Q and a larger isomer shift [37]. Therefore, the Mössbauer spectra may provide information about the coordination environment of oxidized $[2Fe\text{-}2S]^{2+}$ clusters. The one-electron reduced $[2Fe\text{-}2S]^{1+}$ form consists of two distinct valence-trapped sites, an Fe^{III} ion ($S_1 = 5/2$) that is AF-coupled to a Fe^{II} ($S_2 = 2$) yielding an EPR-active $S_{tot} = 1/2$ ground state. The two sites are spectroscopically distinct (Table 1). The local spin of Fe^{II} has positive $\mathbf{A}_{tot}$ (because the spin projection factor is -4/3), whereas for Fe^{III} is parallel to total spin and has negative $\mathbf{A}_{tot}$ (because the spin projection factor is +7/3). This valence trapping is proposed to result from a large AF coupling mediated by the μ_2-sulfide bridges that dominates the opposing double exchange interaction [40]. $[2Fe\text{-}2S]^{+}$clusters have generally trapped valences. The sole exception is a Cys → Ser ligand variant of the [2Fe-2S] ferredoxin from *Clostridium pasteurianum*, which has a valence delocalized $(Fe^{2.5+})_2$ unit [41].

The all ferrous form $[2Fe\text{-}2S]^0$ has been observed in Rieske centers via reduction with a Eu^{II} salt [42]. It has a diamagnetic ground state ($S_{tot} = 0$) that arises from antiparallel alignment of the spins of the two ferrous ions ($S = 2$) as determined by Mössbauer spectroscopy (Table 1).

3.2. [3Fe-4S] clusters

Cuboidal [3Fe-4S] clusters exist in the 1 + and 0 states. The $[3Fe\text{-}4S]^{1+}$ cluster harbors 3 Fe^{III} ions and has a $S_{tot} = 1/2$ ground state that stems from AF coupling of three high-spin ferric ions ($S = 5/2$), as a result of a phenomenon known as spin-frustration [43]. The magnetic-field dependent spectra of $[3Fe\text{-}4S]^{1+}$ clusters exhibit three distinct, yet broad, magnetically split components with $\delta \sim 0.28$ mm/s, and $\Delta E_Q \sim 0.53$ mm/s. The broadness of the subspectra can be rationalized by a distribution of exchange coupling constants, leading to a distribution of admixture of the two low-lying $S_{tot} = 1/2$ states [44,45].

The one-electron reduced $[3Fe\text{-}4S]^0$ form has a $S_{tot} = 2$ ground state resulting from AF coupling of a Fe^{III} ion ($S = 5/2$) to a mixed-valent $(Fe^{2.5+})_2$ pair ($S = 9/2$) [21,43,46]. The delocalized valence states of the two of the Fe ions of the $[3Fe\text{-}4S]^0$ clusters cannot be rationalized

Table 1
Mössbauer and electronic properties of protein-bound Fe/S cofactors at 4.2 K.

Type	Apparent valences	S_{tot}	δ (mm/s)	$\|\Delta E_Q\|$ (mm/s)	D (cm^{-1}), E/D	Ref
$[1Fe]^{3+}_{rubredoxin}$; $[1Fe]^{3+}_{desulforedoxin}$	Fe^{III}; Fe^{III}	5/2; 5/2	0.32; 0.25	0.5; 0.75	1.9, 0.23; 2.2, 0.08	[54,55]
$[1Fe]^{2+}_{rubredoxin}$; $[1Fe]^{2+}_{desulforedoxin}$	Fe^{II}; Fe^{II}	2; 2	0.70; 0.70	3.25; 3.55	7.6, 0.28; -6.0, 0.19	[54,55]
$[2Fe\text{-}2S]^{2+}_{Rieske}$	Fe^{III},Fe^{III}	0	0.24, 0.32	0.32, 0.91		[37]
$[2Fe\text{-}2S]^{2+}_{4Cys}$	Fe^{III},Fe^{III}	0	0.27	0.60		[56]
$[2Fe\text{-}2S]^{1+}_{Rieske}$	Fe^{III},Fe^{II}	1/2	0.31, 0.74	0.63, 3.05		[37]
$[2Fe\text{-}2S]^{1+}_{4Cys}$	Fe^{III},Fe^{II}	1/2	0.35,0.60	0.65,2.70		[56]
$[2Fe\text{-}2S]^{0}$	Fe^{II}-Cys, Fe^{II}-His	0	0.70, 0.81	2.76, 2.32		[42]
$[3Fe\text{-}4S]^{1+}_{cube}$	Fe^{III}, Fe^{III}, Fe^{III}	1/2	0.27	0.63		[43]
$[3Fe\text{-}4S]^{1+}_{linear}$	Fe^{III}, Fe^{III}, Fe^{III}	5/2	0.28, -0.31	nd	1.5–2.5, 0.31	[47]
$[3Fe\text{-}4S]^{0}$	Fe^{III}, {$Fe^{2.5+}$-$Fe^{2.5+}$}	2	0.32, 0.46	0.52, 1.47	-2.5, 0.23	[21]
$[4Fe\text{-}4S]^{3+}$	{Fe^{III}-Fe^{III}}, {$Fe^{2.5+}$-$Fe^{2.5+}$}	1/2	0.29, 0.40	0.88, 1.03		[57]
$[4Fe\text{-}4S]^{2+}$	2x{$Fe^{2.5+}$-$Fe^{2.5+}$}	0	0.42	1.12 (av)		[35]
$[4Fe\text{-}4S]^{1+}$	{Fe^{II}-Fe^{II}}, {$Fe^{2.5+}$-$Fe^{2.5+}$}	1/2*	0.58, 0.49	1.89, 1.32		[35]
$[4Fe\text{-}4S]^{0}$	2x{Fe^{II}-Fe^{II}}	4	0.65	1.51, 2.19	-0.66, 0.17	[58]

by the simple Heisenberg exchange model. The careful analysis of their Mössbauer spectra led to the realization that the valence-delocalized $(Fe^{2.5+})_2$ unit has $S = 9/2$ and the concept of double exchange was introduced to describe this valence delocalization phenomenon [21,43]. The phenomenon of double-exchange was first unequivocally demonstrated for $[3Fe\text{-}4S]^0$ clusters and subsequently shown to play an important role in the electronic structures of many other polynuclear Fe/S clusters (*vide infra*). The 4.2-K/0-T spectrum of the $[3Fe\text{-}4S]^0$ cluster is the superposition of two quadrupole doublets with an intensity ratio 2:1 for the mixed-valent and ferric sites, respectively. The more intense doublet that represents the mixed-valent pair has δ ~0.46 mm/s and ΔE_Q ~1.47 mm/s, whereas the quadrupole doublet corresponding to the Fe^{III} site has δ ~0.32 mm/s and ΔE_Q ~0.52 mm/s. Even in small magnetic fields, the spectrum broadens significantly due to noticeable $\mathbf{B}_{int}$, which is a consequence of the ZFS parameters of the $S_{tot} = 2$ ground spin manifold [21,43].

The cuboidal $[3Fe\text{-}4S]^{1+}$ cluster can reversibly rearrange to adopt a linear configuration with a ground state $S_{tot} = 5/2$ (Table 1) [44,47–49]. The nature of the spin ground state was determined by Mössbauer measurements and can be rationalized by AF interactions of adjacent Fe^{III} ions, resulting in parallel (antiparallel) alignment of the spins of terminal (central) Fe^{III} ions to the $S_{tot} = 5/2$ ground state.

3.3. [4Fe-4S] clusters

Tetranuclear cubane [4Fe-4S] clusters can exist in the four oxidation states 3+, 2+, 1+ and 0 [4,50,51]. They are divided into two subclasses: the high-potential clusters operating in the $[4Fe\text{-}4S]^{3+/2+}$ manifold and the low-potential clusters operating in the $[4Fe\text{-}4S]^{2+/1+}$ manifold [51].

A common theme of these tetranuclear cubane clusters is that they harbor at least one valence-delocalized $(Fe^{2.5+})_2$ pair [4,28,52]. The central and best characterized state of these clusters is the $[4Fe\text{-}4S]^{2+}$ form. $[4Fe\text{-}4S]^{2+}$ clusters have a diamagnetic ground state ($S_{tot} = 0$) [34] that results formally from AF coupling of two valence-delocalized $(Fe^{2.5+})_2$ pairs each having $S = 9/2$ [4,52]. All Fe ions in the cluster are essentially indistinguishable with very similar isomer shift (δ ~0.45 mm/s) and quadrupole splitting parameters (ΔE_Q ~1.0–1.3 mm/s). So far there is only one case of a $[4Fe\text{-}4S]^{2+}$ cluster exhibiting paramagnetism - the cluster of the Δ*nifB* NifEN - that serves as the scaffold for the biosynthesis of the FeMo cofactor in Mo-nitrogenase [53]. This cluster has not yet been studied by Mössbauer spectroscopy.

"Breaking" of the valence delocalization paradigm in $[4Fe\text{-}4S]^{2+}$ clusters may be observed upon binding of alternative ligands (e.g. substrates) to one of the Fe sites of the cluster (changes in coordination number, symmetry, etc.), which can promote (partial) valence trapping in one of the mixed-valent Fe_2 pairs. As a result, a pronounced site differentiation in the Mössbauer spectra of such clusters is observed. This phenomenon was first observed for the citrate-bound form of the $[4Fe\text{-}4S]^{2+}$ cluster in aconitase, in which addition of substrate led to an increase of the isomer shift and quadrupole splitting of one of the Fe ions, indicating a more ferrous character for this site [59]. A similar situation has been observed in the Mössbauer spectra of several "radical SAM" enzymes upon binding of the substrate SAM, to the unique site of a $[4Fe\text{-}4S]^{2+}$ cluster [60–62] and the enzyme ferredoxin:thioredoxin reductase [63]. For the radical-SAM enzymes, SAM binds in a bidentate fashion to the unique, non-cysteinate-coordinated Fe site via the amino and carboxy groups of SAM [64,65]. SAM anchoring to one of the Fe ions increases the coordination number of the so-called 'unique' Fe site and is thought to lead to a lessening of the resonance delocalization within one of the Fe_2 dimers [60]. The different coordination environment (number and type of ligands) may result in changes in the isomer shifts and quadrupole splitting parameters of the Fe ions within the Fe_2 subunit, which are now characteristic now of a (partially) valence-localized pair.

The one-electron reduced $[4Fe\text{-}4S]^{1+}$ state is paramagnetic ($S_{tot} = 1/2$) and the total ground state consists of a diferrous pair $(Fe^{II})_2$ with $S = 4$ (positive *A*'s) AF-coupled to a valence-delocalized $S = 9/2$ mixed-valence pair $(Fe^{2.5+})_2$ (negative *A*'s) [35]. Common values for the isomer shift for the $(Fe^{II})_2$ pair are δ ~ 0.60 mm/s and for the $(Fe^{2.5+})_2$ pair δ ~ 0.49 mm/s (Table 1) [35]. Other total ground spin states have also been observed for $[4Fe\text{-}4S]^{1+}$ clusters (e.g. $S_{tot} = 3/2$, 5/2, and 7/2) [66–68], often in mixtures with the $S_{tot} = 1/2$ state, as a result of perturbations in the coordination environment of the cluster or substitution of the sulfides in the core with selenides [69].

The oxidized $[4Fe\text{-}4S]^{3+}$ form consists of a $(Fe^{III})_2$ pair AF-coupled to a valence-delocalized $(Fe^{2.5+})_2$ pair, yielding a $S_{tot} = 1/2$ ground state. Representative Mössbauer parameters for the $(Fe^{III})_2$ pair are δ ~ 0.29 mm/s and ΔE_Q ~ 0.88 mm/s and for the mixed-valent $(Fe^{2.5+})_2$ pair δ ~ 0.40 mm/s and ΔE_Q ~ 1.03 mm/s (Table 1). The $(Fe^{III})_2$ pair represents the minority spin (positive *A*'s) and the mixed-valent pair the majority spin (negative *A*'s) [57] and due to 'spin canting' the spin coupling configuration within the cluster is proposed to be $S = 7/2$ for the $(Fe^{2.5+})_2$ pair AF-coupled to a $S = 3$ $(Fe^{III})_2$ pair [70].

In a few proteins, such as the Fe-protein of nitrogenase and the activator component of 2-hydroxyglutaryl-CoA dehydratase [23,58,71], the all-ferrous $[4Fe\text{-}4S]^0$ form can be attained employing strong reducing agents. The Mössbauer spectra of the $[4Fe\text{-}4S]^0$ reveal a $S_{tot} = 4$ ground state with weak ZFS parameters (Table 1) and two subspectra with 3:1 intensity ratio. The Mössbauer parameters, δ = 0.71 mm/s and ΔE_Q = 1.80 mm/s (75%) and δ = 0.71 mm/s and ΔE_Q = 2.60 mm/s (25%), are typical of high-spin $Fe^{II}S_4$ sites [23].

4. Novel Fe/S clusters

In the following sections, we describe salient features of two recently described Fe/S clusters, the characterization of which depended significantly on Mössbauer spectroscopy.

4.1. The redox and conformational plasticity of a novel [4Fe-3S] cluster in O_2-tolerant hydrogenases

Aquifex aeolicus is a microaerobic, hyperthermophilic bacterium that owes its name (latin: water maker) to its ability to gain energy by coupling H_2 oxidation to the four-electron O_2 reduction to H_2O [72,73]. A membrane-bound [NiFe] hydrogenase (Hase I) is the first enzyme in this respiration pathway [72]. Hase I is a heterodimeric enzyme consisting of a subunit harboring the dinuclear [NiFe] active site and a second smaller subunit carrying three iron-sulfur clusters, which function as an 'electron relay' to the respective redox partners (i.e. cytochrome b_1). On the basis of their distance from the [NiFe] active site, these are a) a low-potential all-cysteinate ligated [4Fe-4S] cluster (proximal), b) a [3Fe-4S] cluster (medial) and c) a low-potential [4Fe-4S] cluster with three cysteine and one histidine ligands (distal).

Hase I attracted significant attention due to its enhanced O_2-tolerance, in contrast to prototypical hydrogenases of the same subclass that are (ir)reversibly inhibited under aerobic conditions. The ability of Hase I to sustain catalytic activity in the presence of O_2 was reminiscent of a similar behavior reported for the membrane-bound hydrogenase from *Ralstonia eutropha* [75]. Interestingly, both purified enzymes in their as-isolated states exhibit complex Fe/S cluster signals in contrast to the expected g ~2.02 quasi-isotropic EPR signal of a $[3Fe\text{-}4S]^{1+}$ cluster [72,75]. This difference postulated the presence of modified Fe/S centers in these two enzymes. Sequence alignment and site-directed mutagenesis studies revealed that two additional cysteines are involved in the ligation of the proximal [4Fe] cluster [76]. A redox-titration monitored by EPR spectroscopy on the *A. aeolicus* Hase I identified that all three Fe/S clusters are implicated in four single-electron transfer steps [77]. Analysis of the complex magnetic interaction patterns in the EPR spectra supported the hypothesis that the proximal cluster carries out two successive one-electron transitions in a reversible manner and within a small potential range (~150 mV vs NHE) [77]. This analysis revealed that the proximal cluster can access both a superoxidized state (reminiscent of the $[4Fe\text{-}4S]^{3+}$ in HiPIP proteins) and a reduced state (reminiscent of the $[4Fe\text{-}4S]^{1+}$ form in low-potential ferredoxins), and suggested that it may be the first example of a Fe/S cluster physiologically accessing oxidation states separated by two electrons.

To unequivocally address the unprecedented redox conversion of the proximal cluster, Mössbauer spectroscopy was employed so as to probe whether oxidation is indeed contained within the metal center. The system poses a significant challenge for Mössbauer spectroscopy, because it contains in total twelve Fe sites, the contributions of which are significantly overlapping. For a complete and concise characterization of the system, the studies were focused on the two extreme redox states: *chemically superoxidized* (in which the proximal cluster is in its superoxidized state and the other clusters are in their oxidized states, respectively) and *H_2-reduced* (in which the proximal cluster is reduced by two-electrons and the other cofactors are in their one-electron reduced forms). The first definitive evidence that the second redox transition of the proximal cluster is metal-centered was obtained by analysis of the zero-field spectrum recorded at 160 K on the *superoxidized* form of the enzyme (Fig. 4) [77]. This spectrum differed from the one reported for O_2-sensitive hydrogenases by two main features: (i) a substantially higher amount of Fe^{III} that was ascribed to oxidation of the proximal cluster from the (2+)-like state with average valence $Fe^{2.5+}$ to the (3+)-like state ($\delta_{av} = 0.34$ mm/s at 160 K, being in the range of those reported for HiPIP-like cubane clusters) and (ii) a subspectrum corresponding to one Fe ion with an isomer shift of 0.46 mm/s and an unusually large quadrupole splitting $\Delta E_Q = 2.41$ mm/s, indicating an unusual ligand environment. At the same time this study was published, the crystal structure of the superoxidized form of an O_2-tolerant hydrogenase from *Hydrogenothermus marinus* was released [78], revealing a distorted cubane cluster in the proximal position that can be formally described as a [4Fe-3S] cluster, in which one of the inorganic sulfide ligands has been replaced by one of the extra cysteine ligands.

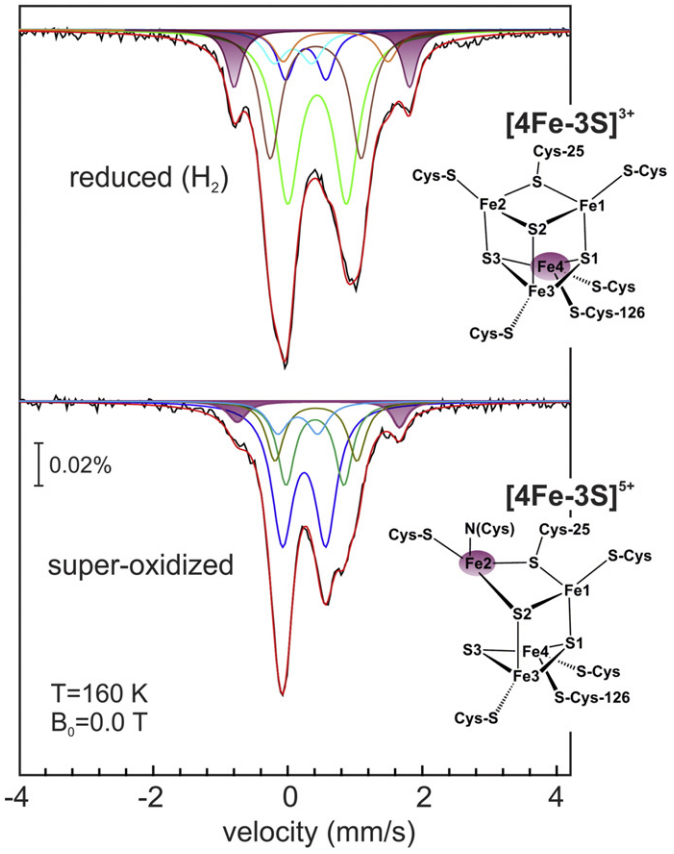

Fig. 4. 160-K/zero-field Mössbauer spectra of the reduced (top) and superoxidized (bottom) form of the *A. aeolicus* Hase I. The so-called unique site has been highlighted with purple shading. The remaining components in the spectra correspond to the relative distribution of ferric, ferrous and mixed-valent sites. Note that the site with unique spectroscopic properties is different in the two redox states. For details refer to ref [74].

In accordance with the predictions from the Mössbauer studies, one of the Fe-sites harbored an atypical amide coordination originating from the tandem CC motif specific for this type of O_2-tolerant enzymes (unique site, top Fig. 4). Further global analysis of the low-temperature (4.2 K) and applied magnetic field Mössbauer spectra, combined with density functional (DFT) calculations and the crystallographic information available, led to the complete characterization of the distribution of Fe valences and spin-coupling schemes for the iron–sulfur clusters in Hase I [74]. In particular, the Mössbauer parameters, and the magnitude and sign of the **A**-tensors surprisingly demonstrate that the electronic structure of the [4Fe-3S] core in its three oxidation states closely resembles that of the conventional [4Fe-4S] clusters, albeit with distinct differences for some individual iron sites, as reflected in the large magnitude of the EFG and the localization of valences (Fig. 4) [74,79].

4.2. The [3Fe]-cluster intermediate in lipoyl synthase (LipA)

The members of the large and emerging superfamily of "radical-SAM" (RS) enzymes [5,80–83] utilize a reduced $[4Fe\text{-}4S]^{1+}$ cluster that is coordinated by a conserved CX_3CX_2C motif to reductively cleave the co-substrate, *S*-adenosyl-L-methionine, to L-methionine and a 5′-deoxyadenos-5′-yl radical (5′-dA•). The 5′-dA• intermediate then reacts with the substrate by abstracting a hydrogen atom from the target C-H bond of the substrate. The RS enzyme lipoyl synthase (LipA) catalyzes the final step in the biosynthesis of the lipoyl cofactor [83,84]. This reaction involves the sequential insertion of two sulfur atoms into the unactivated C-H bonds at C6 and C8 of an octanoyl chain appended to the ε-amino group of a specific lysyl residue of a lipoyl carrier protein,

one of which is the H protein of the glycine cleavage system [85]. A combination of site-directed mutagenesis studies, and Mössbauer- and EPR-spectroscopic experiments, together with metal analyses, revealed that LipA harbors two spectroscopically indistinguishable $[4Fe\text{-}4S]^{2+}$ clusters in its as-isolated state [86]. The first [4Fe-4S] cluster is coordinated by the signature CX_3CX_2C motif of the RS enzymes and is used for reductive generation of the 5′-dA•. The second [4Fe-4S] cluster, denoted as the auxiliary cluster, is coordinated by the three cysteines of a CX_4CX_5C motif, which is conserved amongst LipAs from various species, as well as a serine found in a conserved RSSY motif [87]. It was proposed that the auxiliary [4Fe-4S] cluster in LipA is the source of the sulfur atoms to be inserted into the substrate, because formation of product does not require an exogenous sulfur source and because of the similarity of LipA to the RS enzyme biotin synthase (BioB), which catalyzes insertion of one sulfur atom into two aliphatic C-H bonds at C6 and C9 of dethiobiotin [88]. Importantly, BioB also harbors two Fe/S clusters, a [4Fe-4S] and a [2Fe-2S] cluster [38,96]. The [2Fe-2S] cluster in BioB is the source of the inserted sulfur [61,89,90].

The reaction mechanism of LipA is proposed to proceed in two distinct steps [91,92]. The first step involves generation of 5′-dA• at the RS [4Fe-4S] cluster, followed by abstraction of a hydrogen atom from C6 of the substrate's octanoyl fatty-acyl chain by the 5′-dA•. Subsequent attack of the ensuing substrate radical on one of the μ_3-sulfido ligands of the auxiliary cluster yields the 6-mercapto-octanoyl intermediate [84]. The second step involves generation of another 5′-dA• from a second molecule of SAM at the RS [4Fe-4S] cluster, attack of the 5′-dA• on C8 of the monothiolated intermediate to generate the C8 substrate radical, and attack of the latter on a second sulfide of the auxiliary Fe/S cluster to form the lipoyl cofactor.

The proposed monothiolated intermediate in the LipA reaction was recently trapped and characterized by reacting *Escherichia coli* (*Ec*) LipA in the presence of the octanoyl-H protein-derived peptide substrate with one equivalent of SAM in the presence of dithionite reductant [93]. Under these SAM-limited conditions the reaction is only allowed to proceed to the monothiolated intermediate form, in which the octanoyl substrate is found to be chemically crosslinked to LipA via an iron-sulfur cluster. Mössbauer spectroscopic characterization of the intermediate reveals that the auxiliary [4Fe-4S] cluster is converted to a 3Fe cluster with spectroscopic properties strikingly similar to those observed for reduced, cuboidal $[3Fe\text{-}4S]^0$ clusters (*vide infra*) [93]. When this intermediate is reacted further with an additional equivalent of SAM, formation of lipoyl product is observed with concomitant disassembly of the [3Fe] cluster–containing intermediate and conversion to Fe^{II} in solution, thus demonstrating its kinetic and chemical competence. Alternatively, the same [3Fe] cluster species with identical properties could also be observed in LipAs from *Ec* and from *Thermus thermophilus* by using an 8,8,8-trideuterated octanoyl substrate isotopolog [93], which is known to suppress formation of lipoyl product, due to a large deuterium kinetic isotope effect on C8-H cleavage [91].

The 4.2-K/53-mT Mössbauer spectrum of the as-isolated *Ec* LipA control sample exhibits a quadrupole doublet with parameters $\delta = 0.45$ mm/s and $\Delta E_Q = 1.18$ mm/s, characteristic of $[4Fe\text{-}4S]^{2+}$ clusters (Fig. 5A). By contrast, the spectrum of the monothiolated intermediate is markedly different and contains components that are dependent on the presence or absence of a weak 53-mT magnetic field (Fig. 5B and C), suggesting the presence of a new species with a paramagnetic, integer-spin ground state. The [0-53] mT difference spectrum (Fig. 5D), in which the contribution of the other components is cancelled, reflects the field strength dependence of the spectrum of the intermediate. The zero-field reference spectrum of the paramagnetic intermediate [Fig. 5E, vertical bars, generated by adding back the 53-mT reference spectrum (Fig. 5D, solid line)] consists of two quadrupole doublets in a 2:1 intensity ratio with parameters typical of a mixed-valent $(Fe^{2.5+})_2$ pair and a Fe^{III} site, respectively. The 2:1 intensity ratio and the typical Mössbauer parameters suggest a trinuclear cluster composed of a high-spin Fe^{III} ($S = 5/2$) coupled to a mixed-valent

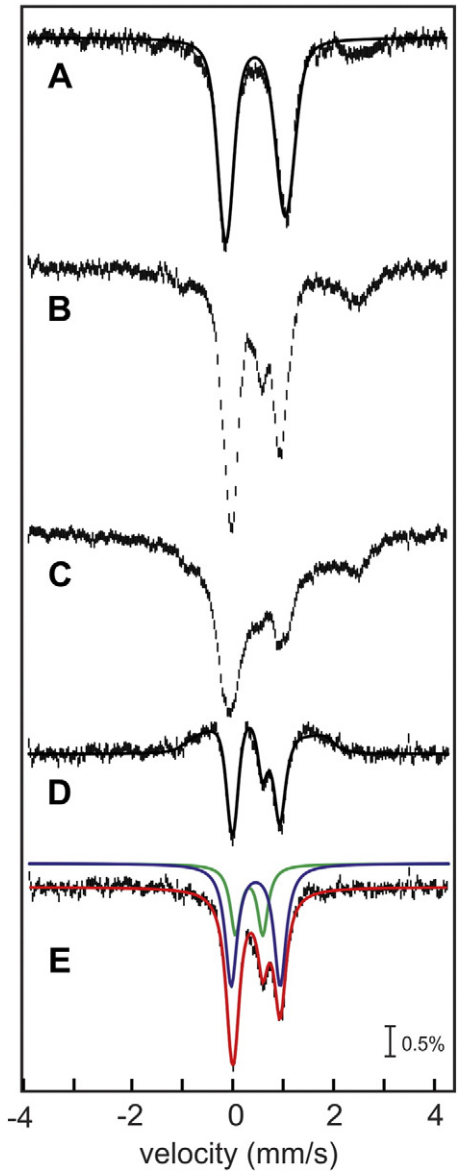

Fig. 5. Mössbauer spectra of the as-purified LipA at 53 mT (A), of the cross-linked monothiolated intermediate at zero-field (B) and at 53 mT (C). The [0-53] mT difference spectrum demonstrates the presence of a [3Fe] paramagnetic cluster (D) and the generated reference quadrupole doublet spectrum of the [3Fe] cluster shows the 2:1 stoichiometry. Applied field is parallel to the γ beam. Adapted from ref [93].

$(Fe^{2.5+})_2$ pair ($S = 9/2$). The parameters of the LipA [3Fe] cluster intermediate are strikingly similar to those of cuboidal $[3Fe\text{-}4S]^0$ clusters, which have a $S_{tot} = 2$ ground state arising from AF coupling of the Fe^{III} site to the $(Fe^{2.5+})_2$. We proposed that formation of the [3Fe] cluster involves attack of the substrate C-6• on one of the sulfide ligands of the auxiliary $[4Fe\text{-}4S]^{2+}$ cluster. In this process, one of the electrons of the lone electron pair of the attacked sulfur is formally used to form the new C-S bond, while the other is added to one of the $(Fe^{2.5+})_2$ units to formally create a $(Fe^{II})_2$ unit. We designate this cluster as $[4Fe\text{-}3S\text{-}1RS]^{2+}$. In terms of its electronic structure, we anticipate that it contains a mixed-valent $(Fe^{2.5+})_2$ unit and a $(Fe^{II})_2$ unit, as in reduced $[4Fe\text{-}4S]^{1+}$ clusters. Note that the cluster has one fewer negative charge, because one of the bridging sulfides has been replaced with the thiolate of the 6-mercaptooctanoyl intermediate. In order to reach the experimentally observed [3Fe]-cluster with one Fe^{III} and one $(Fe^{2.5+})_2$ unit, the cluster needs to lose one Fe^{II} and an additional electron. We designate this cluster as $[3Fe\text{-}3S\text{-}1RS]^+$. Note that this conversion is formally analogous to the oxidative disassembly of $[4Fe\text{-}4S]^{2+}$ clusters to $[3Fe\text{-}4S]^+$

clusters. Loss of Fe^{II} and an electron without further structural rearrangement to yield an approximately cuboidal geometry for the [3Fe-3S-1RS]$^{+}$ cluster would also be in accord with the experimentally observed electronic structure, because the necessary orbital pathways for double exchange within the $(Fe^{2.5+})_2$ unit and magnetic superexchange between the three Fe ions would be present in that geometry.

The other species contributing to the Mössbauer spectra include `regular' [4Fe-4S]$^{2+}$ clusters and [4Fe-4S]$^{2+}$ clusters with two site-differentiated sites (SAM- or methionine-bound), attributed to the RS cluster, as well as high-spin Fe^{II}, which emanates from the Fe^{II} liberated upon disassembly of the auxiliary cluster [93].

5. Characterization of Fe/S clusters by whole-cell/organelle Mössbauer spectroscopy

The type and stoichiometry of Fe/S cofactors are typically determined on purified proteins, i.e. under *in vitro* conditions. Various Fe/S cluster forms, however, can often easily interconvert or degrade, thus raising the question of whether the Fe/S cofactor composition in purified Fe/S proteins is a consequence of the purification procedure. Mössbauer spectroscopy on samples of whole cells or whole organelles may provide additional, complementary information about composition and distribution of the Fe-containing species. However, this approach also has some caveats. In addition to the features of the (Fe/S) protein to be studied, Mössbauer spectroscopy is approximately equally sensitive to *all other* ^{57}Fe-labeled centers contained in the sample, and therefore the spectra typically exhibit several broad components reflecting the "background" of numerous Fe species. Thus, identification of authentic signals associated with the protein of interest may be difficult. Comparison of spectra of whole-cell samples before and after overexpression of the target protein often aids in the analysis of the spectra and identification of the signals of the protein to be studied. It is important, however, to keep in mind that the distribution of background Fe species may change in response to overexpression of the target protein. In the following, we summarize selected studies on the application of this methodology.

The fumarate nitrate reductase (FNR) transcription regulator acts as an O_2-sensor in *Ec* [94]. It was shown by Mössbauer spectroscopy on the purified FNR regulator that it harbors a [4Fe-4S] cluster, which upon exposure to O_2 converts to a [2Fe-2S] cluster. However, it was not known whether this process occurs *in vivo*. By employing Mössbauer spectroscopy on whole cells containing overexpressed FNR, it was demonstrated that the [4Fe-4S]$^{2+}$ to [2Fe-2S]$^{2+}$ interconversion upon exposure to O_2 indeed takes place *in vivo*. In addition, the [4Fe-4S]$^{2+}$ cluster is partly regenerated upon removal of O_2. The spectra of cells in which FNR was not induced were used as a reference for other Fe containing proteins that can be present at high amounts and were then subtracted from the spectra of the FNR overexpressing cells, thus separating the contribution of solely the Fe/S clusters of the transcription factor.

Biotin synthase (BioB) is a RS enzyme that catalyzes the ultimate step in the biosynthesis of biotin, *viz* the insertion of sulfur into the unactivated C6-H and C9-H bonds of dethiobiotin. Before it was firmly established that BioB harbors one [4Fe-4S] and one [2Fe-2S] cluster, it was not clear whether the [2Fe-2S] cluster observed upon purification under anaerobic conditions is an authentic cofactor of BioB, or whether it is the degradation product of a [4Fe-4S] cluster [38,95,96]. Two independent whole-cell Mössbauer studies on BioB demonstrated that the [2Fe-2S] cluster is indeed formed *in vivo* [97,98].

The RS enzyme pyruvate formate lyase activating enzyme (PFL-AE) abstracts the pro-*S* hydrogen atom from a specific glycine residue on PFL using a SAM-derived 5′-dA•, yielding an O_2-sensitive glycyl radical [99,100]. It was shown by Mössbauer spectroscopy that anaerobically purified PFL-AE contains a mixture of Fe/S cluster types ([2Fe-2S]$^{2+}$, cuboidal [3Fe-4S]$^{+}$, linear [3Fe-4S]$^{+}$, and [4Fe-4S]$^{2+}$) [44,101], which upon treatment with dithionite convert to a mixture of [4Fe-4S]$^{1+/2+}$. To examine the potential physiological relevance of the interconversion of [4Fe-4S]$^{2+}$ to [2Fe-2S]$^{2+}$ *in vivo*, i.e. regulation of PFL activity in response to O_2 levels, Mössbauer spectroscopy on whole cells expressing PFL-AE demonstrated that the [4Fe-4S]$^{2+}$-to-[2Fe-2S]$^{2+}$ interconversion occurs *in vivo* [102]. In addition, it was observed that the [4Fe-4S]$^{2+}$ cluster in the cells has a partially valence-localized Fe_2 unit, suggesting binding of a small molecule to the unique non-cysteine-coordinated site of the [4Fe-4S] cluster.

Mössbauer spectroscopy can be combined with EPR spectroscopy and analytical methods (inductively coupled plasma atomic emission spectroscopy, ICP-AES) in order to study the Fe speciation in cells and organelles. Such an approach has been adopted for the study of the Fe distribution in mitochondria, which are the 'kernels' for the cellular Fe trafficking [103]. This combined study demonstrated how Fe is mobilized to be inserted into proteins and how the relative concentrations of Fe-containing proteins (heme, non-heme and Fe/S-containing proteins) are modulated in yeast cells during the different metabolic phases (respiration, fermentation).

6. Outlook and conclusions

Mössbauer spectroscopy has unarguably set the stage for understanding the electronic structure of polynuclear Fe/S clusters, which has been itself pivotal for establishing the fundamental mechanisms that dictate their conformational, electronic and redox plasticity. It is an invaluable tool and by far the most informative method when the nuclearity and redox states of Fe/S cofactors in uncharacterized proteins need to be determined. The importance of this technique is particularly accentuated in studies of novel Fe/S cofactors that go against hitherto accepted paradigms occurring in more 'classical' clusters and allows for the characterization of the electronic structure of these cofactors, otherwise inaccessible by other methods. Though the complexity of the Mössbauer spectra increases with increasing the number of Fe species, selective ^{57}Fe labeling and coupling to other spectroscopic techniques such as EPR, EXAFS, and resonance Raman spectroscopies, offers a unique handle for the study of Fe/S clusters.

References

[1] H. Beinert, Iron-sulfur proteins: ancient structures, still full of surprises, J. Biol. Inorg. Chem. 5 (2000) 2–15.
[2] R. Cammack, Iron-sulfur clusters in enzymes – themes and variations, Adv. Inorg. Chem. 38 (1992) 281–322.
[3] D.C. Johnson, D.R. Dean, A.D. Smith, M.K. Johnson, Structure, function, and formation of biological iron-sulfur clusters, Annu. Rev. Biochem. 74 (2005) 247–281.
[4] H. Beinert, R.H. Holm, E. Münck, Iron-sulfur clusters: Nature's modular, multipurpose structures, Science 277 (1997) 653–659.
[5] J.B. Broderick, B.R. Duffus, K.S. Duschene, E.M. Shepard, Radical S-adenosylmethionine enzymes, Chem. Rev. 114 (2014) 4229–4317.
[6] R. Lill, Function and biogenesis of iron-sulphur proteins, Nature 460 (2009) 831–838.
[7] J. Meyer, Iron-sulfur protein folds, iron-sulfur chemistry, and evolution, J. Biol. Inorg. Chem. 13 (2008) 157–170.
[8] D.C. Rees, J.B. Howard, The interface between the biological and inorganic worlds: iron-sulfur metalloclusters, Science 300 (2003) 929–931.
[9] T.A. Rouault, Biogenesis of iron-sulfur clusters in mammalian cells: new insights and relevance to human disease, Dis. Model. Mech. 5 (2012) 155–164.
[10] P.J. Kiley, H. Beinert, The role of Fe-S proteins in sensing and regulation in bacteria, Curr. Opin. Microbiol. 6 (2003) 181–185.
[11] M.F. White, Structure, function and evolution of the XPD family of iron-sulfur-containing 5′- > 3′ DNA helicases, Biochem. Soc. Trans. 37 (2009) 547–551.
[12] E. Münck, Mössbauer spectroscopy of proteins: Electron carriers, in: F. Sidney, P. Lester (Eds.), Methods enzymol, Academic Press, 1978, pp. 346–379.
[13] P. Gütlich, E. Bill, A.X. Trautwein, Mössbauer spectroscopy and transition metal chemistry:fundamentals and applications, Springer-Verlag, Berlin Heidelberg, 2011.
[14] N.D. Lanz, T.L. Grove, C.B. Gogonea, K.H. Lee, C. Krebs, S.J. Booker, RlmN and AtsB as models for the overproduction and characterization of radical SAM proteins, Methods Enzymol. 516 (2012) 125–152.
[15] A.X. Trautwein, E. Bill, E.L. Bominaar, H. Winkler, Iron-containing proteins and related analogs – complementary Mössbauer, EPR, and magnetic susceptibility studies, Struct. Bond. 78 (1991) 1–95.
[16] N.N. Greenwood, T.C. Gibb, Mössbauer spectroscopy, Chapman and Hall, London, 1971.
[17] E. Münck, Physical methods in bioinorganic chemistry, University Science Books, New York, 2000.
[18] P. Gütlich, R. Link, A.X. Trautwein, Mössbauer spectroscopy and transition metal chemistry, Springer, Berlin, 1978.

[19] V. Schünemann, H. Winkler, Structure and dynamics of biomolecules studied by Mössbauer spectroscopy, Rep. Prog. Phys. 63 (2000) 263–353.
[20] A. Abragam, B. Bleaney, Electron paramagnetic resonance of transition ions, Oxford University Press, Oxford, 1970.
[21] V. Papaefthymiou, J.J. Girerd, I. Moura, J.J.G. Moura, E. Münck, Mössbauer study of *D. gigas* ferredoxin-II and spin-coupling model for the Fe_3S_4 cluster with valence delocalization, J. Am. Chem. Soc. 109 (1987) 4703–4710.
[22] I. Moura, J.J.G. Moura, B.H. Huynh, H. Santos, J. Legall, A.V. Xavier, Ferredoxin from *Methanosarcina barkeri* – evidence for the presence of a 3-iron center, Eur. J. Biochem. 126 (1982) 95–98.
[23] S.J. Yoo, H.C. Angove, B.K. Burgess, M.P. Hendrich, E. Münck, Mössbauer and integer-spin EPR studies and spin-coupling analysis of the $[4Fe\text{-}4S]^0$ cluster of the Fe protein from *Azotobacter vinelandii* nitrogenase, J. Am. Chem. Soc. 121 (1999) 2534–2545.
[24] L. Noodleman, C.Y. Peng, D.A. Case, J.M. Mouesca, Orbital interactions, electron delocalization and spin coupling in iron-sulfur clusters, Coord. Chem. Rev. 144 (1995) 199–244.
[25] O. Kahn, Molecular magnetism, VCH, New York, 1993.
[26] A. Bencini, D. Gatteschi, Electron paramagnetic resonance of exchange coupled systems, Springer-Verlag, Berlin, 1990.
[27] C.H. Wu, W. Jiang, C. Krebs, J.A. Stubbe, YfaE, a ferredoxin involved in diferric-tyrosyl radical maintenance in *Escherichia coli* ribonucleotide reductase, Biochemistry 46 (2007) 11577–11588.
[28] E.L. Bominaar, S.A. Borshch, J.J. Girerd, Double-exchange and vibronic coupling in mixed-valence systems – electronic-structure of $[Fe4S4]^{3+}$ clusters in high-potential iron protein and related models, J. Am. Chem. Soc. 116 (1994) 5362–5372.
[29] G. Blondin, J.J. Girerd, Interplay of electron exchange and electron-transfer in metal polynuclear complexes in proteins or chemical-models, Chem. Rev. 90 (1990) 1359–1376.
[30] J.J. Girerd, Electron-transfer between magnetic ions in mixed-valence binuclear systems, J. Chem. Phys. 79 (1983) 1766–1775.
[31] L. Noodleman, D.A. Case, J.M. Mouesca, B. Lamotte, Valence electron delocalization in polynuclear iron-sulfur clusters, J. Biol. Inorg. Chem. 1 (1996) 177–182.
[32] T.V. Harris, R.K. Szilagyi, Iron–sulfur bond covalency from electronic structure calculations for classical iron–sulfur clusters, J. Comput. Chem. 35 (2014) 540–552.
[33] J.M. Mouesca, L. Noodleman, D.A. Case, B. Lamotte, Spin-densities and spin coupling in iron-sulfur clusters - a New analysis of hyperfine coupling-constants, Inorg. Chem. 34 (1995) 4347–4359.
[34] D.P.E. Dickson, C.E. Johnson, R. Cammack, M.C.W. Evans, D.O. Hall, K.K. Rao, Mössbauer effect in high-potential iron-sulfur protein from *Chromatium* – evidence for state of iron atoms, Biochem. J. 139 (1974) 105–108.
[35] P. Middleton, D.P.E. Dickson, C.E. Johnson, J.D. Rush, Interpretation of Mössbauer-spectra of 4-iron ferredoxin from *Bacillus stearothermophilus*, Eur. J. Biochem. 88 (1978) 135–141.
[36] R.H. Sands, W.R. Dunham, Spectroscopic studies on two-iron ferredoxins, Q. Rev. Biophys. 7 (1974) 443–504.
[37] J.A. Fee, K.L. Findling, T. Yoshida, R. Hille, G.E. Tarr, D.O. Hearshen, W.R. Dunham, E.P. Day, T.A. Kent, E. Münck, Purification and characterization of the rieske iron-sulfur protein from *Thermus thermophilus* – evidence for a [2Fe-2S] cluster having Non-cysteine ligands, J. Biol. Chem. 259 (1984) 124–133.
[38] F. Berkovitch, Y. Nicolet, J.T. Wan, J.T. Jarrett, C.L. Drennan, Crystal structure of biotin synthase, an S-adenosylmethionine-dependent radical enzyme, Science 303 (2004) 76–79.
[39] M.M. Dicus, A. Conlan, R. Nechushtai, P.A. Jennings, M.L. Paddock, R.D. Britt, S. Stoll, Binding of histidine in the $(Cys)_3(His)_1$-coordinated [2Fe − 2S] cluster of human mitoNEET, J. Am. Chem. Soc. 132 (2010) 2037–2049.
[40] T. Glaser, B. Hedman, K.O. Hodgson, E.I. Solomon, Ligand K-edge X-ray absorption spectroscopy: A direct probe of ligand-metal covalency, Acc. Chem. Res. 33 (2000) 859–868.
[41] C. Achim, M.P. Golinelli, E.L. Bominaar, J. Meyer, E. Münck, Mössbauer study of Cys56Ser mutant 2Fe ferredoxin from *Clostridium pasteurianum*: Evidence for double exchange in an $Fe_2S_2^+$ cluster, J. Am. Chem. Soc. 118 (1996) 8168–8169.
[42] E.J. Leggate, E. Bill, T. Essigke, G.M. Ullmann, J. Hirst, Formation and characterization of an all-ferrous Rieske cluster and stabilization of the $[2Fe\text{-}2S]^0$ core by protonation, Proc. Natl. Acad. Sci. U. S. A. 101 (2004) 10913–10918.
[43] T.A. Kent, B.H. Huynh, E. Münck, Iron-sulfur proteins – spin-coupling model for 3-iron clusters, Proc. Natl. Acad. Sci. U. S. A. 77 (1980) 6574–6576.
[44] C. Krebs, T.F. Henshaw, J. Cheek, B.H. Huynh, J.B. Broderick, Conversion of 3Fe-4S to 4Fe-4S clusters in native pyruvate formate-lyase activating enzyme: Mössbauer characterization and implications for mechanism, J. Am. Chem. Soc. 122 (2000) 12497–12506.
[45] Y. Sanakis, A.L. Macedo, I. Moura, J.J.G. Moura, V. Papaefthymiou, E. Münck, Evidence for antisymmetric exchange in cuboidal $[3Fe\text{-}4S]^+$ clusters, J. Am. Chem. Soc. 122 (2000) 11855–11863.
[46] E. Münck, T.A. Kent, Structure and magnetism of iron-sulfur clusters in proteins, Hyperfine Interact. 27 (1986) 161–172.
[47] M.C. Kennedy, T.A. Kent, M. Emptage, H. Merkle, H. Beinert, E. Münck, Evidence for the formation of a linear [3Fe-4S] cluster in partially unfolded aconitase, J. Biol. Chem. 259 (1984) 4463–4471.
[48] K. Jones, C.M. Gomes, H. Huber, M. Teixeira, P. Wittung-Stafshede, Formation of a linear 3Fe-4S cluster in a seven-iron ferredoxin triggered by polypeptide unfolding, J. Biol. Inorg. Chem. 7 (2002) 357–362.
[49] B. Zhang, S. Bandyopadhyay, P. Shakamuri, S.G. Naik, B.H. Huynh, J. Couturier, N. Rouhier, M.K. Johnson, Monothiol glutaredoxins Can bind linear $[Fe_3\text{-}S_4]^+$ and $[Fe_4\text{-}S_4]^{2+}$ clusters in addition to $[Fe_2\text{-}S_2]^{2+}$ clusters: spectroscopic characterization and functional implications, J. Am. Chem. Soc. 135 (2013) 15153–15164.
[50] E. Bill, Iron-sulfur clusters-new features in enzymes and synthetic models, Hyperfine Interact. 205 (2012) 139–147.
[51] W.V. Sweeney, J.C. Rabinowitz, Proteins containing 4Fe-4S clusters – an overview, Annu. Rev. Biochem. 49 (1980) 139–161.
[52] M. Kröckel, M. Grodzicki, V. Papaefthymiou, A.X. Trautwein, A. Kostikas, Tuning of electron delocalization in polynuclear mixed-valence clusters by super-exchange and double exchange, J. Biol. Inorg. Chem. 1 (1996) 173–176.
[53] K. Rupnik, C.C. Lee, Y.L. Hu, M.W. Ribbe, B.J. Hales, $[4Fe4S]^{2+}$ clusters exhibit ground-state paramagnetism, J. Am. Chem. Soc. 133 (2011) 6871–6873.
[54] C. Schulz, P.G. Debrunner, Rubredoxin, a simple iron-sulfur protein: its spin hamiltoman and hyperfine parameters, J. Phys. Colloq. 37 (1976) (C6-153-C156-158).
[55] I. Moura, B.H. Huynh, R.P. Hausinger, J. Le Gall, A.V. Xavier, E. Münck, Mössbauer and EPR studies of desulforedoxin from *Desulfovibrio gigas*, J. Biol. Chem. 255 (1980) 2493–2498.
[56] E. Münck, J.C.M. Tsibris, I.C. Gunsalus, P.G. Debrunner, Mössbauer parameters of putidaredoxin and its selenium analog, Biochemistry 11 (1972) 855–863.
[57] P. Middleton, D.P.E. Dickson, C.E. Johnson, J.D. Rush, Interpretation of the Mössbauer-spectra of the high-potential iron protein from *Chromatium*, Eur. J. Biochem. 104 (1980) 289–296.
[58] M. Hans, W. Buckel, E. Bill, Spectroscopic evidence for an all-ferrous $[4Fe\text{-}4S]^0$ cluster in the superreduced activator of 2-hydroxyglutaryl-CoA dehydratase from *Acidaminococcus fermentans*, J. Biol. Inorg. Chem. 13 (2008) 563–574.
[59] M.H. Emptage, T.A. Kent, M.C. Kennedy, H. Beinert, E. Münck, Mössbauer and electron paramagnetic resonance studies of activated aconitase – development of a localized valence state at a subsite of the 4Fe-4S cluster on binding of citrate, Proc. Natl. Acad. Sci. U. S. A. 80 (1983) 4674–4678.
[60] C. Krebs, W.E. Broderick, T.F. Henshaw, J.B. Broderick, B.H. Huynh, Coordination of adenosylmethionine to a unique iron site of the [4Fe-4S] of pyruvate formate-lyase activating enzyme: A Mössbauer spectroscopic study, J. Am. Chem. Soc. 124 (2002) 912–913.
[61] G.N.L. Jameson, M.M. Cosper, H.L. Hernandez, M.K. Johnson, B.H. Huynh, Role of the [2Fe-2S] cluster in recombinant *Escherichia coli* biotin synthase, Biochemistry 43 (2004) 2022–2031.
[62] K.H. Lee, L. Saleh, B.P. Anton, C.L. Madinger, J.S. Benner, D.F. Iwig, R.J. Roberts, C. Krebs, S.J. Booker, Characterization of RimO, a New member of the methylthiotransferase subclass of the radical SAM superfamily, Biochemistry 48 (2009) 10162–10174.
[63] E.M. Walters, R. García Serres, G.N.L. Jameson, D.A. Glauser, F. Bourquin, W. Manieri, P. Schurmann, M.K. Johnson, B.H. Huynh, Spectroscopic characterization of site-specific $[Fe_4S_4]$ cluster chemistry in ferredoxin: thioredoxin reductase: Implications for the catalytic mechanism, J. Am. Chem. Soc. 127 (2005) 9612–9624.
[64] J.L. Vey, J. Yang, M. Li, W.E. Broderick, J.B. Broderick, C.L. Drennan, Structural basis for glycyl radical formation by pyruvate formate-lyase activating enzyme, Proc. Natl. Acad. Sci. U. S. A. 105 (2008) 16137–16141.
[65] C.J. Walsby, W. Hong, W.E. Broderick, J. Cheek, D. Ortillo, J.B. Broderick, B.M. Hoffman, Electron-nuclear double resonance spectroscopic evidence that S-adenosylmethionine binds in contact with the catalytically active $[4Fe\text{-}4S]^+$ cluster of pyruvate formate-lyase activating enzyme, J. Am. Chem. Soc. 124 (2002) 3143–3151.
[66] R.E. Duderstadt, P.S. Brereton, M.W.W. Adams, M.K. Johnson, A pure $S = 3/2$ $[Fe_4S_4]^+$ cluster in the A33Y variant of *Pyrococcus furiosus* ferredoxin, FEBS Lett. 454 (1999) 21–26.
[67] M. Boll, G. Fuchs, G. Tilley, F.A. Armstrong, D.J. Lowe, Unusual spectroscopic and electrochemical properties of the 2[4Fe-4S] ferredoxin of *Thauera aromatica*, Biochemistry 39 (2000) 4929–4938.
[68] M. Heinnickel, R. Agalarov, N. Svensen, C. Krebs, J.H. Golbeck, Identification of F_X in the heliobacterial reaction center as a [4Fe-4S] cluster with an $S = 3/2$ ground spin state, Biochemistry 45 (2006) 6756–6764.
[69] J. Meyer, J.M. Moulis, Replacement of sulfide by selenide in the [4Fe-4S] clusters of the ferredoxin from *Clostridium pasteurianum*, Biochem. Biophys. Res. Commun. 103 (1981) 667–673.
[70] J.M. Mouesca, B. Lamotte, Iron-sulfur clusters and their electronic and magnetic properties, Coord. Chem. Rev. 178 (1998) 1573–1614.
[71] H.C. Angove, S.J. Yoo, B.K. Burgess, E. Münck, Mössbauer and EPR evidence for an all-ferrous Fe_4S_4 cluster with $S = 4$ in the Fe protein of nitrogenase, J. Am. Chem. Soc. 119 (1997) 8730–8731.
[72] M. Brugna-Guiral, P. Tron, W. Nitschke, K.O. Stetter, B. Burlat, B. Guigliarelli, M. Bruschi, M.T. Giudici-Orticoni, [NiFe] hydrogenases from the hyperthermophilic bacterium *Aquifex aeolicus:* properties, function, and phylogenetics, Extremophiles 7 (2003) 145–157.
[73] M. Guiral, T. Aubert, M.T. Giudici-Orticoni, Hydrogen metabolism in the hyperthermophilic bacterium *Aquifex aeolicus*, Biochem. Soc. Trans. 33 (2005) 22–24.
[74] M.E. Pandelia, D. Bykov, R. Izsak, P. Infossi, M.T. Giudici-Orticoni, E. Bill, F. Neese, W. Lubitz, Electronic structure of the unique [4Fe-3S] cluster in O_2-tolerant hydrogenases characterized by ^{57}Fe Mössbauer and EPR spectroscopy, Proc. Natl. Acad. Sci. U. S. A. 110 (2013) 483–488.
[75] M. Saggu, C. Teutloff, M. Ludwig, M. Brecht, M.E. Pandelia, O. Lenz, B. Friedrich, W. Lubitz, P. Hildebrandt, F. Lendzian, R. Bittl, Comparison of the membrane-bound [NiFe] hydrogenases from *R. eutropha* H16 and *D. vulgaris* Miyazaki F in the oxidized ready state by pulsed EPR, Phys. Chem. Chem. Phys. 12 (2010) 2139–2148.
[76] T. Goris, A.F. Wait, M. Saggu, J. Fritsch, N. Heidary, M. Stein, I. Zebger, F. Lendzian, F.A. Armstrong, B. Friedrich, O. Lenz, A unique iron-sulfur cluster is crucial for oxygen tolerance of a [NiFe]-hydrogenase, Nat. Chem. Biol. 7 (2011) 310–318.
[77] M.E. Pandelia, W. Nitschke, P. Infossi, M.T. Giudici-Orticoni, E. Bill, W. Lubitz, Characterization of a unique [FeS] cluster in the electron transfer chain of the oxygen

tolerant [NiFe] hydrogenase from *Aquifex aeolicus*, Proc. Natl. Acad. Sci. U. S. A. 108 (2011) 6097–6102.
[78] Y. Shomura, K.S. Yoon, H. Nishihara, Y. Higuchi, Structural basis for a [4Fe-3S] cluster in the oxygen-tolerant membrane-bound [NiFe]-hydrogenase, Nature 479 (2011) 253–256.
[79] J.M. Mouesca, J.C. Fontecilla-Camps, P. Amara, The structural plasticity of the proximal [4Fe-3S] cluster is responsible for the O_2 tolerance of membrane-bound [NiFe] hydrogenases, Angew. Chem. Int. Ed. 52 (2013) 2002–2006.
[80] P.A. Frey, A.D. Hegeman, F.J. Ruzicka, The radical SAM superfamily, Crit. Rev. Biochem. Mol. Biol. 43 (2008) 63–88.
[81] H.J. Sofia, G. Chen, B.G. Hetzler, J.F. Reyes-Spindola, N.E. Miller, Radical SAM, a novel protein superfamily linking unresolved steps in familiar biosynthetic pathways with radical mechanisms: functional characterization using new analysis and information visualization methods, Nucleic Acids Res. 29 (2001) 1097–1106.
[82] S.J. Booker, Anaerobic functionalization of unactivated C-H bonds, Curr. Opin. Chem. Biol. 13 (2009) 58–73.
[83] S.J. Booker, R.M. Cicchillo, T.L. Grove, Self-sacrifice in radical S-adenosylmethionine proteins, Curr. Opin. Chem. Biol. 11 (2007) 543–552.
[84] N.D. Lanz, S.J. Booker, The role of iron-sulfur clusters in the biosynthesis of the lipoyl cofactor, in: T.A. Rouault (Ed.), Iron-sulfur clusters in chemistry and biology, De Gruyter, Berlin, 2014.
[85] R.M. Cicchillo, S.J. Booker, Mechanistic investigations of lipoic acid biosynthesis in *Escherichia coli:* Both sulfur atoms in lipoic acid are contributed by the same lipoyl synthase polypeptide, J. Am. Chem. Soc. 127 (2005) 2860–2861.
[86] R.M. Cicchillo, K.H. Lee, C. Baleanu-Gogonea, N.M. Nesbitt, C. Krebs, S.J. Booker, *Escherichia coli* lipoyl synthase binds two distinct [4Fe-4S] clusters per polypeptide, Biochemistry 43 (2004) 11770–11781.
[87] J.E. Harmer, M.J. Hiscox, P.C. Dinis, S.J. Fox, A. Iliopoulos, J.E. Hussey, J. Sandy, F.T. Van Beek, J.W. Essex, P.L. Roach, Structures of lipoyl synthase reveal a compact active site for controlling sequential sulfur insertion reactions, Biochem. J. 464 (2014) 123–133.
[88] C.J. Fugate, J.T. Jarrett, Biotin synthase: insights into radical-mediated carbon-sulfur bond formation, Biochim. Biophys. Acta 1824 (2012) 1213–1222.
[89] B.T.S. Bui, D. Florentin, F. Fournier, O. Ploux, A. Mejean, A. Marquet, Biotin synthase mechanism: on the origin of sulphur, FEBS Lett. 440 (1998) 226–230.
[90] A.M. Taylor, S. Stoll, R.D. Britt, J.T. Jarrett, Reduction of the [2Fe-2S] cluster accompanies formation of the intermediate 9-mercaptodethiobiotin in *Escherichia coli* biotin synthase, Biochemistry 50 (2011) 7953–7963.
[91] R.M. Cicchillo, D.F. Iwig, A.D. Jones, N.M. Nesbitt, C. Baleanu-Gogonea, M.G. Souder, L. Tu, S.J. Booker, Lipoyl synthase requires two equivalents of S-adenosyl-L-methionine to synthesize one equivalent of lipoic acid, Biochemistry 43 (2004) 6378–6386.
[92] P. Douglas, M. Kriek, P. Bryant, P.L. Roach, Lipoyl synthase inserts sulfur atoms into an octanoyl substrate in a stepwise manner, Angew. Chem. Int. Ed. 45 (2006) 5197–5199.
[93] N.D. Lanz, M.E. Pandelia, E.S. Kakar, K.H. Lee, C. Krebs, S.J. Booker, Evidence for a catalytically and kinetically competent enzyme-substrate cross-linked intermediate in catalysis by lipoyl synthase, Biochemistry 53 (2014) 4557–4572.
[94] C.V. Popescu, D.M. Bates, H. Beinert, E. Münck, P.J. Kiley, Mössbauer spectroscopy as a tool for the study of activation/inactivation of the transcription regulator FNR in whole cells of *Escherichia coli*, Proc. Natl. Acad. Sci. U. S. A. 95 (1998) 13431–13435.
[95] N.B. Ugulava, K.K. Surerus, J.T. Jarrett, Evidence from Mössbauer spectroscopy for distinct $[2Fe\text{-}2S]^{2+}$ and $[4Fe\text{-}4S]^{2+}$ cluster binding sites in biotin synthase from *Escherichia coli*, J. Am. Chem. Soc. 124 (2002) 9050–9051.
[96] M.M. Cosper, G.N.L. Jameson, H.L. Hernandez, C. Krebs, B.H. Huynh, M.K. Johnson, Characterization of the cofactor composition of *Escherichia coli* biotin synthase, Biochemistry 43 (2004) 2007–2021.
[97] R. Benda, B. Tse Sum Bui, V. Schünemann, D. Florentin, A. Marquet, A.X. Trautwein, Iron-sulfur clusters of biotin synthase *in vivo*: a Mössbauer study, Biochemistry 41 (2002) 15000–15006.
[98] M.M. Cosper, G.N.L. Jameson, M.K. Eidsness, B.H. Huynh, M.K. Johnson, Recombinant *Escherichia coli* biotin synthase is a $[2Fe\text{-}2S]^{2+}$ protein in whole cells, FEBS Lett. 529 (2002) 332–336.
[99] C.J. Walsby, D. Ortillo, J. Yang, M.R. Nnyepi, W.E. Broderick, B.M. Hoffman, J.B. Broderick, Spectroscopic approaches to elucidating novel iron-sulfur chemistry in the "Radical-SAM" protein superfamily, Inorg. Chem. 44 (2005) 727–741.
[100] K.A. Shisler, J.B. Broderick, Glycyl radical activating enzymes: structure, mechanism, and substrate interactions, Arch. Biochem. Biophys. 546 (2014) 64–71.
[101] J.B. Broderick, T.F. Henshaw, J. Cheek, K. Wojtuszewski, S.R. Smith, M.R. Trojan, R.M. McGhan, A. Kopf, M. Kibbey, W.E. Broderick, Pyruvate formate-lyase-activating enzyme: strictly anaerobic isolation yields active enzyme containing a $[3Fe\text{-}4S]^{+}$ cluster, Biochem. Biophys. Res. Commun. 269 (2000) 451–456.
[102] J. Yang, S.G. Naik, D.O. Ortillo, R. García Serres, M. Li, W.E. Broderick, B.H. Huynh, J.B. Broderick, The iron-sulfur cluster of pyruvate formate-lyase activating enzyme in whole cells: cluster interconversion and a valence-localized $[4Fe\text{-}4S]^{2+}$ state, Biochemistry 48 (2009) 9234–9241.
[103] J.G. Morales, G.P. Holmes-Hampton, R. Miao, Y.S. Guo, E. Münck, P.A. Lindahl, Biophysical characterization of iron in mitochondria isolated from respiring and fermenting yeast, Biochemistry 49 (2010) 5436–5444.